In situ rolling circle amplification Förster resonance energy transfer (RCA-FRET) for washing-free real-time single protein imaging

Laura Francés-Soriano,[1,2] Mattias Leino,[3] Marcelina Cardoso Dos Santos,[2] Daniel Kovacs,[4] K. Eszter Borbas,[4] Ola Söderberg,[3] and Niko Hildebrandt[1,2]*

1 nanoFRET.com, Laboratoire COBRA (Chimie Organique, Bioorganique, Réactivité et Analyse), Université de Rouen Normandie, CNRS, INSA, 76821 Mont-Saint-Aignan, France

2 Institute for Integrative Biology of the Cell (I2BC), Université Paris-Saclay, CNRS, CEA, 91405 Orsay Cedex, France

3 Department of Pharmaceutical Biosciences, Uppsala University, Biomedical Center, 75124 Uppsala, Sweden

4 Department of Chemistry, Ångström Laboratory, Uppsala University, 75120 Uppsala, Sweden

E-mail: niko.hildebrandt@univ-rouen.fr

Abstract

Fluorescence signal enhancement via isothermal nucleic acid amplification is an important approach for sensitive imaging of intra or extracellular nucleic acid or protein biomarkers. Rolling circle amplification (RCA) is frequently applied for fluorescence *in situ* imaging but faces limitations concerning multiplexing, dynamic range, and the required multiple washing steps before imaging. Here, we show that Förster Resonance Energy Transfer (FRET) between fluorescent dyes and between lanthanide complexes (Ln) and dyes that hybridize to β-actin-specific RCA products in HaCaT cells can afford washing-free imaging of single β-actin proteins. Proximity-dependent FRET could be monitored directly after or during (real-time monitoring) dye or Ln DNA probe incubation and efficiently distinguish between photoluminescence from β-actin-specific RCA and DNA probes freely diffusing in solution or non-specifically attached to cells. Moreover, time-gated FRET imaging with the Ln-dye FRET pairs efficiently suppressed sample autofluorescence and improved the signal-to-background ratio. Our results present an important proof-of-concept of RCA-FRET imaging with a strong potential to advance *in situ* RCA toward easier sample preparation, higher-order multiplexing, autofluorescence-free detection, and increased dynamic range by real-time monitoring of *in situ* RCA.

Keywords: FRET, proximity ligation, lanthanides, time-gating, imaging, autofluorescence.

In situ proximity ligation assays (*in situ* PLA) that use rolling circle amplification (RCA) of DNA for fluorescence signal amplification have become an important biosensing method for analyzing single proteins and protein interactions both at the single cell level and in heterogeneous cell populations, *e.g.*, in tissue sections used for clinical diagnostics.[1,2] In *in situ* PLA, binding of pairs of antibodies labeled with specific DNA oligonucleotides (PLA-probes) templates the ligation of circularization oligonucleotides into circular DNA molecules. The formation of a circular molecule is dependent on that the PLA-probes bind in close proximity. Utilizing the oligonucleotides of the PLA-probes as primers, the circular DNA molecule will be amplified by RCA, creating a long single-stranded RCA product (RCP). Individual RCPs can be visualized by the addition of fluorescent detection oligonucleotides that hybridize to the RCP concatemer.[3] Owing to the significant signal amplification, even very low protein levels can be detected for each individual cell by fluorescence imaging because each RCP formed on a single protein or protein interaction results in an individual and bright fluorescence spot. Since their initial development,[4] *in situ* PLA have been advanced concerning efficiency, multiplexing, and dynamic range.[5–7] However, multiplexing has been limited to three colors (three different fluorescent dyes)[6] and increasing the dynamic range requires the use of different concentrations of DNA circles and different fluorescent labels.[5] Moreover, background fluorescence, caused by autofluorescence and free fluorescent detection oligos, interferes with the RCP fluorescence. Hence, to reduce background, several washing steps are applied after RCP-hybridization of the fluorescent detection oligonucleotides to remove excess.

An efficient approach to design homogeneous (*i.e.*, washing-free) assays in solution is FRET (Förster resonance energy transfer).[8] FRET assays are washing-free because donors and acceptors must be in close proximity (usually closer than ~10 nm) to engage in FRET. Thus, donors and acceptors that are free in solution do not emit FRET signals and can be distinguished from the target-bound donors and acceptors without separation. In addition, measuring the emission of the acceptor upon excitation of the donor results in a larger spectral separation between excitation and emission wavelengths compared to the Stokes shift separation in a single-fluorophore system, which results in further background (autofluorescence or excitation light) reduction. The combination of lanthanide complexes as FRET donors and time-gated (TG) photoluminescence (PL) detection into TG-FRET[9] has been implemented into homogeneous immunoassays more than 20 years ago and commercialized under the names of *HTRF* (homogeneous time-resolved

fluorescence), *LANCE* (lanthanide chelate excite), or *TRACE* (time-resolved amplified cryptate emission) for biomolecular screening and clinical diagnostics.[10–14] More recently, we have translated TG-FRET into homogeneous nucleic acid detection,[15–17] and, in particular, into homogeneous RCA-TG-FRET assays for the detection of single-point mutations in DNA or the quantification of microRNAs from extracts of human plasma, cells, and tissues.[18–20] In addition to the washing-free assay format (no separation steps), high sensitivity (sub-femtomolar limits of detection), and high specificity (single nucleotide mismatches), RCA-TG-FRET can significantly enhance multiplexing by combining both the color (wavelength) and the time (lifetime) components of PL into higher-order spectrotemporal multiplexing.[21] The combination of RCA and FRET in solution was also accomplished by dye-dye donor-acceptor pairs, which allowed the use of the more conventional steady-state or continuous-wave (CW) detection (instead of TG) but such dye-dye FRET is limited in multiplexing and the suppression of autofluorescence background.[22,23] Despite the advantages in liquid-phase assays, RCA-FRET has never been implemented into imaging on the single-protein level in cells or tissues, most probably due to the more challenging conditions of the cellular environment and fixation and permeabilization procedures.

To demonstrate the applicability of RCA-FRET for analysis within cells, we utilized immuno-RCA,[24] which reports the abundance of antibodies in the cells, rather than *in situ* PLA that reports the abundance of proximity between bound PLA-probes. By reducing the complexity of the biological recognition from single protein interaction to single protein binding, we could focus on the adequate analysis of the different FRET signals. For this proof-of-concept study, we used different dye-dye and lanthanide-dye FRET pairs that were coupled to specific detection oligonucleotides for RCPs generated with immuno-RCA targeting β-actin in HaCaT cells. Single-actin-specific RCPs could be visualized in CW imaging for all three dyes (Cy3.5, AlexaFluor 647 – AF647, and Texas Red) and in TG imaging for two different Tb complexes and one Eu complex. The brightest detection oligonucleotides were selected for RCA-FRET, which resulted in efficient Cy3.5-to-AF647 RCA-CW-FRET and Tb-to-Cy3.5 RCA-TG-FRET. The proximity-dependent FRET signal allowed us to efficiently distinguish between PL from RCPs and PL from detection oligonucleotides freely diffusing in solution or non-specifically attached to cells, which could be exploited for bright actin-specific imaging without the three washing steps that were necessary for simple fluorescence (without FRET).[7] TG-FRET could also be used for real-time monitoring of detection oligonucleotide hybridization to the actin-specific RCPs. This proof-of-concept system

showed that both CW FRET and TG FRET are suitable for *in situ* PLA, do not require washing steps after detection oligo incubation with the RCP, and open various possibilities concerning faster sample preparation, improved multiplexing, increased dynamic range, reduced background caused by autofluorescence and non-specific binding, and real-time *in situ* monitoring of RCA.

MATERIALS AND METHODS

Materials. All DNA oligonucleotides (including reactive groups and/or conjugated organic dyes Cy3.5, AlexaFluor 647, and Texas Red) were purchased from Eurogentec or Biomers and used after purification by HPLC. N-hydroxysuccinimide (NHS)-functionalized Lumi4-Tb (Tb-NHS) was provided by Lumiphore, Inc. (Berkeley, USA).[25] Azide-functionalized Tb and Eu complexes (Tb_x-azide and Eu_x-azide) were synthesized as previously described.[26] Sequences of the padlock DNA and the detection oligonucleotides are shown in **Table 1**. The HaCaT cell line (epidermal keratinocyte cell line from adult human skin) was a kind gift from Carl-Henrik Heldin.

Table 1. Sequences of padlock probe and detection oligonucleotides.

Name	Sequence (5' → 3')
Padlock DNA	CTA TTA GCG TC**C AGT GAA TGC GAG TCC GTC TAA GAG AGT AGT ACA GCA GCC** GTC AAG AGT GTC TAG TTC TGT CAT ATT TAA GCG TCT TAA
Tb-**DNA_1**	Tb **C AGT GAA TGC GAG TCC GTC T**
Cy3.5-**DNA_2**	Cy3.5 **AA GAG AGT AGT ACA GCA GCC**
AF647-**DNA_1**	AF647 **C AGT GAA TGC GAG TCC GTC T**
Texas Red-**DNA_1**	Texas Red **C AGT GAA TGC GAG TCC GTC T**
Eu_x-**DNA_1**	Eu_x **C AGT GAA TGC GAG TCC GTC T**
Tb_x-**DNA_1**	Tb_x **C AGT GAA TGC GAG TCC GTC T**

Optical spectroscopy. UV/Vis absorption spectroscopy was carried out on a LAMBDA 35 UV/VIS spectrophotometer (PerkinElmer). PL emisssion spectra were recorded on a Xenius XM fluorometer (SAFAS).

Lanthanide-DNA bioconjugation. DNA-Tb bioconjugation was carried out by following a previously described protocol.[16] Briefly, a 16-fold excess of Tb-NHS was stirred with the amino-functionalized oligonucleotides (Eurogentec) in 100 nM carbonate buffer (pH 9.0) overnight at 4 °C. Then, the Tb-oligo conjugates were purified three times with HEPES buffer (100 mM, pH 7.4) by Zeba Spin Desalting Columns (7 KDa MWCO). Tb and DNA concentrations were

determined by their absorption in HEPES buffer at 340 nm (ε_{Tb} = 26000 $M^{-1}\cdot cm^{-1}$) and 260 nm (ε_{DNA} = 190000 $M^{-1}\cdot cm^{-1}$), respectively. The concentration of the Tb-oligo1 solution after conjugation was 12 µM. DNA-Tb_x and DNA-Eu_x bioconjugation was carried out by mixing 0.2 mM Tb_x or Eu_x, which contained a reactive azide group, with 0.02 mM DBCO-modified oligonucleotides (Biomers) in 100 mM potassium phosphate buffer (pH 6.5). The 100 µl reaction was incubated at RT overnight, followed by a 7K MWCO Zeba spin column centrifugation to remove unconjugated Tb_x or Eu_x. The samples were then examined using 10% TBE urea gel, stained with SYBR Gold (Thermo Fisher Scientific) for 15 min. The gel showed that all oligonucleotides had been conjugated and no unconjugated oligonucleotides could be detected. Concentration of the DNA-Tb_x and DNA-Eu_x conjugates were determined by Nanodrop 3000 (Molecular Devices).

Determination of FRET parameters. The overlap integrals (*J*) for the Cy3.5-Alexa647 pair and Tb-Cy3.5 pair were calculated using equation 1:[27]

$$J = \int_{\lambda_1}^{\lambda_2} I_D(\lambda) \cdot \varepsilon_A(\lambda) \cdot \lambda^4 d\lambda \qquad (1)$$

where I_D is the area-normalized (to unity between λ_1 and λ_2) donor emission spectrum, ε_A is the acceptor molar extinction coefficient (in $M^{-1}cm^{-1}$), and λ is the wavelength of light. λ_1 and λ_2,fixed to 565 nm and 710 nm for the Cy3.5-Alexa647 pair and to 450 nm and 700 nm for the Tb-Cy3.5 pair. The Förster distances (R_0) for both donor-acceptor pairs were obtained by using equation 2:[27]

$$R_0 = 0.021 \cdot (\kappa^2 \cdot \Phi_D \cdot n^{-4} \cdot J)^{1/6} \quad \text{(in nm)} \qquad (2)$$

where κ^2 is the orientation factor, which depends upon the relative orientations of the transition dipole moments of donor emission and acceptor absorption and the dynamically averaged value 2/3 was assumed, Φ_D is the donor PL quantum yield (Φ_D(Cy3.5) = 0.30 ± 0.05, Φ_D(Tb) = 0.7 ± 0.1), and n = 1.35 the refractive index of the aqueous buffer solution. Φ_D(Tb) and n were taken from previous work concerning Tb-based FRET sensing in solution.[17] Φ_D(Cy3.5) was roughly estimated based on a value of ~15% (specifications of the provider Cytiva) and a strong quantum yield increase when Cy3 dyes were conjugated to the terminus of DNA.[28] Notably, photophysical conditions of the DNA-probes hybridized to RCPs in fixed and permeabilized cells can be significantly different. However, an estimation was sufficient for evaluating the possibility of *in situ* RCA-FRET.

Preparation of fixed and permeabilized cells and actin immuno-RCA. HaCaT cells were grown in high glucose Dulbecco′s Modified Eagle′s Medium (DMEM) containing 10% fetal bovine serum (FBS) and passaged every 2 to 3 days using trypsin ethylenediaminetetraacetic acid (EDTA). Cells were seeded, grown overnight, fixed in 4% paraformaldehyde (PFA) for 15 min on ice, washed three times in phosphate buffered saline (PBS) for 10 min, dried, and then stored in a freezer until use. For actin immuno-RCA, cells were permeabilized with Triton100 (0.2%) for 10 min, blocked with "Intercept (TBS) Protein-Free Blocking Buffer" (LI-COR) for 1 h, and incubated with anti-actin AB_1 (Santa-Cruz sc-47778) overnight at 4 °C. Then, DNA-labeled secondary AB_2 (Donkey-anti-mouse antibody, Jackson 715-005-151), conjugated with 5´-aldehyde-AAAAAAAAAA GACGCTAATA GTTAAGACGCTT (IDT) using S-HyNic (VWR S-1002-105) according to previously published protocol[29] and diluted in blocking buffer, was added and incubated for 1 h at 37 °C. Afterwards, 0.125 µM of padlock DNA (s3a2 padlock) were added and ligated (over the DNA sequence on AB_2) for 30 min at 37 °C in 1x T4 ligation buffer containing 0.25 mg/mL bovine serum albumin (BSA) and 0.05 U/µL T4 ligase. RCA was performed for 1.5 h at 37°C in 1x phi29 polymerase buffer (Fermentas) containing 0.25 mg/mL BSA, 7.5 ng/mL polyA, 0.25 mM dNTP mix, and 0.5 U/µL phi29 polymerase. Afterwards, the chamber slides (8 well Lab-Tek Chamber Slides, Merck) were dipped in 70 % ethanol, dried, and sent for fluorescence imaging (note that all preparation steps mentioned above were performed at Uppsala University, whereas the RCP hybridization with detection probes and imaging were performed at Université Paris-Saclay).

Hybridization of detection oligonucleotides to RCP. For dye-to-dye FRET (as shown in **Figure 2**), tris-buffered saline (TBS, 150 mM NaCl, 50 mM Tris-Cl, pH=7.6) containing the detection oligonucleotides AF647-DNA_1 (0.025 µM) and Cy3.5-DNA_2 (0.025 µM) and 0.25 mg/mL BSA was prepared. Then, fixed HaCaT cells were incubated with 30 µL of the previously prepared reagent solution at 36.5 °C. After 30 min, the solution was removed and cells were washed three times for 5 minutes in TBS buffer at room temperature. Then, 30 µL of TBS was added to the well and the slide was covered with a glass cover slip such that the cells could be imaged through the cover slip. Control images were acquired from cells incubated with equivalent mixtures but without detection oligonucleotides. For Tb-to-dye FRET, different buffers and procedures were applied. All hybridization steps were performed on HaCaT cells fixed in chamber slides that were imaged from the bottom (no cover slip was necessary). The first experiments (as

shown in **Figure 3**) used the same reagent solution as mentioned above for dye-to-dye FRET with the exception that AF647-DNA_1 was replaced by Tb-DNA_1. Also, the incubation procedure was the same with the exception that no TBS was added after washing. The real-time *in situ* hybridization monitoring experiments with Tb-to-Cy3.5 FRET (as shown in **Figure 4**) used Hank's Balanced Salt Solution (HBSS) buffer instead of TBS. After addition of the reagent solution to the chamber slides, they were immediately placed into a heating sample holder in the microscope, such that the temperature of 36.5 °C was stable over the entire imaging period of 2 h. The final Tb-to-dye FRET experiments (as shown in **Figure 5**) used HBSS buffer for the reagent solution and only 15 min of incubation (instead of 30 min). Before imaging, the reagent solution was removed and no further washing steps were applied.

CW and TG PL imaging. Microscope images were acquired using a wide-field, inverted microscope (Olympus IX71) equipped with a UV laser (349 nm, 300 Hz, Nd:YLF, Triton, Spectra Physics) for pulsed excitation (Tb, Tb_x, and Eu_x excitation in TG imaging), X-Cite 120Q mercury source (Lumen Dynamics) continuous source for CW excitation at 12.5% (15 W lamp power) max. intensity (dye excitation in CW imaging), and an intensified CCD camera (ICCD, PI-MAX3, Princeton Instruments) for detection. PL signals were collected with a high numerical aperture (NA = 1.35) immersion oil objective (UPLSAPO 60× O, Olympus).

For CW dye-to-dye FRET, the following filter and mirror (all from Semrock) specifications were used: *Donor excitation:* 510/42 (~ 510 ± 21 nm) bandpass filter for Cy3.5 excitation and 596 nm dichroic mirror for excitation/emission separation; *Acceptor excitation:* 620/14 (~ 620 ± 7 nm) bandpass filter for AF647 excitation and 649 nm dichroic mirror for excitation/emission separation; *Donor emission:* 605/15 (~ 605 ± 8 nm) bandpass filter for Cy3.5 imaging; *Acceptor emission:* 720/13 (~ 720 ± 7 nm) bandpass filter for AF647 imaging.

For TG Tb-to-dye FRET, the following filter and mirror (all from Semrock) specifications were used: *Donor excitation:* 349 nm laser without additional filter and 405 nm dichroic mirror for excitation/emission separation; *Acceptor excitation:* 578/16 (~ 578 ± 8 nm) bandpass filter for Cy3.5 excitation and 596 nm dichroic mirror for excitation/emission separation; *Donor emission:* 542/20 (~ 542 ± 10 nm) bandpass filter for Tb imaging; *Acceptor emission:* 660/10 (~ 660 ± 5 nm) bandpass filter for Cy3.5 imaging.

Acquisition settings (WinView camera control software) were generally fixed to the following parameters: *CW imaging (PL and DIC):* 10 acquisitions with 300 ms excitation, 6 V gain. *TG imaging:* 400 gates per image (GPI), 1 acquisition (Ac), 100 V gain, 10 µs delay, 2 ms gate. Background was acquired on bare slides or cover slips (without cells) with the same acquisition settings and subtracted from the raw images.

RESULTS AND DISCUSSION

Principle of RCA-FRET imaging. The immuno-RCA proof-of-concept system (**Figure 1a**) consisted of an anti-β-actin antibody (AB_1) that binds to actin on permeabilized HaCaT cells followed by binding of secondary anti-mouse antibody (AB_2) that contained a DNA oligonucleotide with a specific sequence for hybridizing a DNA padlock probe to initiate RCA after ligating the padlock nick. The resulting single RCPs per single β-actin were visualized by incubation with RCP-specific detection oligos. These oligos were labeled with dyes or lanthanide complexes for CW or TG PL detection of the fluorophores alone or the FRET-pairs. To evaluate the imaging performance of the single fluorophores and to demonstrate the applicability to various organic dyes and lanthanide complexes, we designed detection oligos (*cf.* **Table 1** for DNA sequences) with three different commercial organic dyes (Cy3.5, AF647, and Texas Red) and three different lanthanide complexes (Tb,[25] Tb_x,[26] and Eu_x,[26] see **Supporting Figure S1** for chemical structures). Although all detection oligonucleotides resulted in actin-specific RCP imaging (**Supporting Figure S2**), AF647, Cy3.5, and Tb provided the brightest PL signals and we selected those three detection oligos for further FRET investigations.

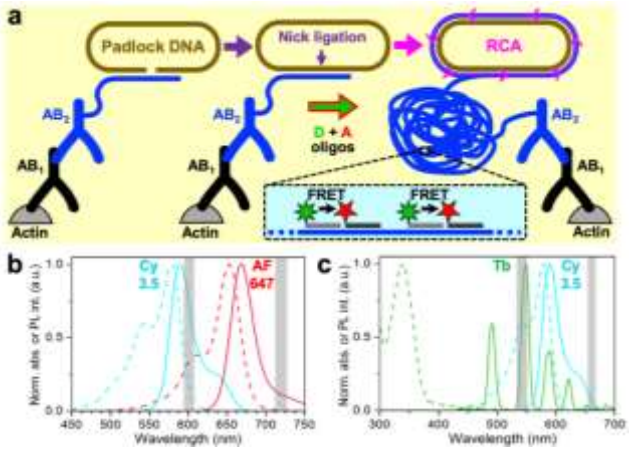

Figure 1. a: Principle of actin specific RCA-FRET detection. After AB_1 binding to actin, DNA-functionalized AB_2 binds AB_1 and a circular DNA is formed by DNA-padlock hybridization. After nick ligation (*via* T4 ligase), AB_2-DNA serves as a primer to initiate RCA (via phi29 polymerase and dNTPs). Incubation with FRET donor and acceptor detection oligonucleotides (D + A oligos) results in hybridization to the RCP and concomitant FRET from D to A due to their close proximity inside the RCP. **b:** Absorption (dashed lines) and PL (solid lines) spectra of Cy3.5 (CW-FRET donor) and AF647 (CW-FRET acceptor) detection oligos and transmission spectral regions (in gray) of transmission band pass filters used for Cy3.5 and AF647 detection in CW microscopy experiments. **c:** Absorption (dashed lines) and PL (solid lines) spectra of Tb (TG-FRET donor) and Cy3.5 (TG-FRET acceptor) detection oligos and transmission spectral regions (in gray) of transmission band pass filters used for Tb and Cy3.5 detection in TG microscopy experiments.

Figure 1b (Cy3.5-AF647 CW-FRET pair) and **Figure 1c** (Tb-Cy3.5 TG-FRET pair) show the absorption and emission spectra of donors and acceptors and the transmission regions of the bandpass filters used for their detection in microscopy. The spectral overlap of donor emission and acceptor absorption resulted in overlap integrals (**Equation 1**) of J (Cy3.5-AF647) = $1.28 \cdot 10^{16}$ $M^{-1}cm^{-1}$ and J (Tb-Cy3.5) = $6.24 \cdot 10^{15}$ $M^{-1}cm^{-1}$ and Förster distances (donor-acceptor distance with 50 % FRET efficiency, **Equation 2**) of R_0(Cy3.5-AF647) = 6.4 ± 0.4 nm and R_0(Tb-Cy3.5) = 6.5 ± 0.4 nm. Based on our previous experience in designing detector oligonucleotides for efficient hybridization and FRET inside the coiled RCP structure,[18,19,21,30] we functionalized all fluorophores on the 3' ends of a 20-nucleotide DNA (*cf.* **Table 1**). With an estimated distance of ~0.33 nm between two bases within double-stranded DNA,[31] the donor-acceptor distances inside the detector oligonucleotide-bound RCPs should be approximately 6.6 nm, which is close to the R_0 values (50% FRET efficiency) and should result in significant change in donor and acceptor PL intensities and lifetimes for efficient FRET imaging.

RCA-CW-FRET from Cy3.5 to AF647. To demonstrate the feasibility of RCA-FRET for conventional organic dyes and conventional PLA conditions,[3] we prepared a solution, containing both Cy3.5-DNA_2 and AF647-DNA_1 donor and acceptor detection oligonucleotides, that was incubated for 30 min (36.5 °C) with the β-actin-specific-RCP-containing fixed HaCaT cells. Afterwards, the solution was removed and the cells were washed three times with TBS buffer to remove the excess of non-hybridized oligonucleotides. To avoid dye photobleaching, the slide was protected from the light during the manipulation time. Fresh TBS was added on the washed cells and a 170 µm thick cover slip was placed on top. For imaging on the inverted microscope, the slide was turned (cover slip on the bottom). Direct excitation of Cy3.5 and AF647 as well as FRET excitation of AF647 via Cy3.5 resulted in the characteristic staining patterns of actin-activated

RCPs in permeabilized and fixed cells, as shown by the many bright target spots (**Figure 2a**).[7] Because FRET spots can only be detected when Cy3.5 and AF647 are in close proximity (<10 nm), which means attached to the same RCP, the FRET image suppresses all fluorescence that originates from non-specific Cy3.5 and/or AF647 signals (*e.g.*, probes that were not washed off the cells). This advantage becomes much more evident when no washing was performed and the cells were imaged directly after 30 min incubation with both detection oligonucleotides (**Figure 2b**). In this case, both directly excited Cy3.5 and AF647 resulted in strong fluorescence background of dye-oligonucleotides that were not hybridized to the RCPs whereas the FRET images show only those fluorescence spots that result from β-actin-specific immuno-RCA. Thus, the *in situ* RCA-FRET approach can completely avoid any repetitive and time-consuming washing steps and results in specific detection signals with improved signal-to-noise ratios due to the strongly reduced background fluorescence, which may become even more important for strongly autofluorescent samples, such as tissue sections.

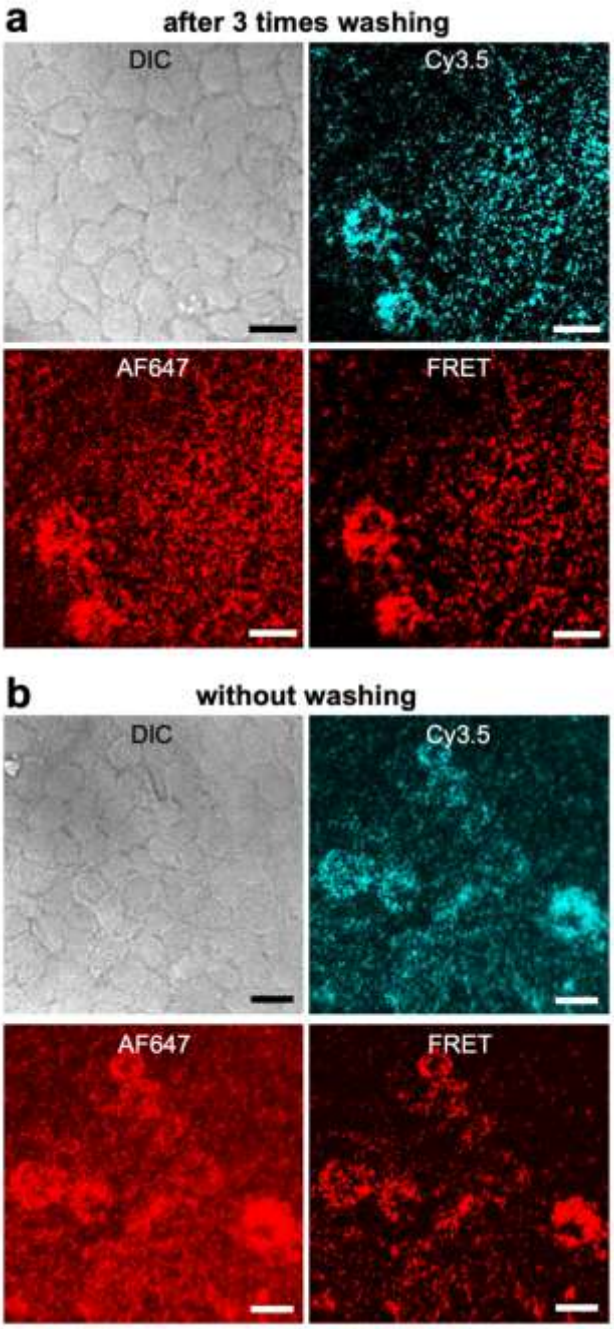

Figure 2. *In situ* RCA-FRET imaging (**a:** after washing; **b:** without washing) of individual actin-activated immuno RCPs on HaCaT cells incubated with Cy3.5 donor probes and AF647 acceptor probes. Cy3.5: excitation: 510±21 nm, emission: 605±8 nm; AF647: excitation: 620±7 nm, emission: 720±7 nm; FRET: excitation: 510±21 nm, emission: 720±7 nm. Imaging conditions: 10 times 300 ms, gain: 6 V, lamp power: 15 W. Scale bars: 20 µm. DIC/PL overlay image can be found in **Supporting Figure S3**.

RCA-TG-FRET from Tb to Cy3.5. Although autofluorescence of endogenous biological components is not strong in most fixed cells, in contrast to, *e.g.*, formalin-fixed paraffin-embedded

or glutaraldehyde fixed tissue sections, we wanted to demonstrate the proof-of-concept of utilizing TG-FRET, which can become extremely beneficial for investigating highly autofluorescent tissue or *in vivo* samples.[32–34] Thus, we applied Tb-to-Cy3.5 FRET and TG imaging to the same samples that were used for Cy3.5-to-AF647 FRET. Surprisingly, first experiments using the exact same sample preparation conditions as for CW FRET did not result in any Tb PL. Because Tb is very stable in various buffers (including TBS) and has been applied to many in-solution assays and for live cell and *in vivo* imaging without significant PL quenching,[20,35–38] we assumed that the fixation procedure combined with incubation of the fixed cells with an aqueous buffer (*i.e.*, the TBS buffer washed out some of the PFA fixative) caused the Tb PL quenching. We found that removal of TBS from the cells (*i.e.*, without addition of fresh TBS after the three usual washing steps) and direct imaging resulted in bright PL signals (**Figure 3**) of Tb (in TG detection mode), Cy3.5 (in CW detection mode), and Tb-Cy3.5 FRET (in TG detection mode). Because only RCPs hybridized with both Tb and Cy3.5 probes (close Tb-Cy3.5 proximity) could lead to FRET, the FRET channel (TG imaging of Cy3.5 PL) resulted in significantly better contrast of the specific RCP signals with higher signal-to-background ratios than the Tb (TG) or Cy3.5 (CW) images (**Supporting Figure S5**). Comparing the bottom left area of the Cy3.5 (CW) and FRET (TG) images (**Figure 3**, bottom right), one can appreciate that the RCP-specific PL spots in the FRET image (pink frame) appear at a similar brightness than those from the cells on the top and bottom right (yellow frames), whereas the Cy3.5 images show strong differences in brightness of those RCP spots. Such differences can result from inconsistent non-specific DNA probe attachment from one cell to the other. Control experiments with only Tb probes, only Cy3.5 probes, and no probes (**Supporting Figure S6**) demonstrated that the detection channels were specific to their probes and that FRET could only be detected when both probes were present.

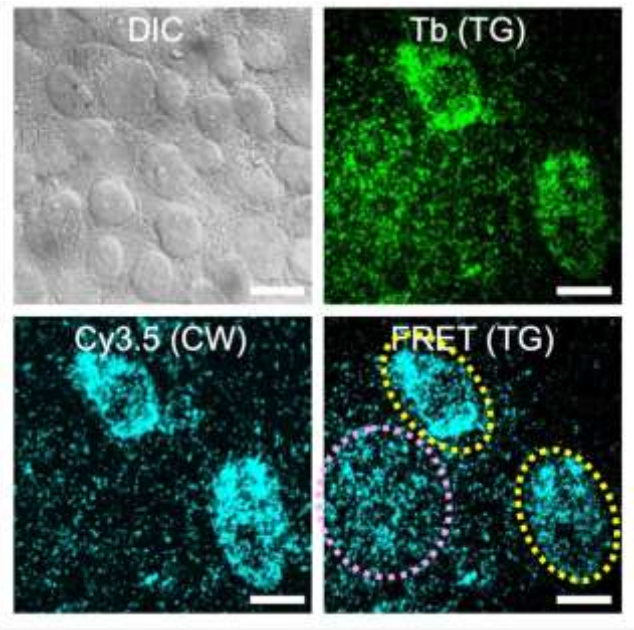

Figure 3: *In situ* RCA-FRET imaging of individual actin-activated immuno-RCPs on HaCaT cells incubated with Tb donor probes and Cy3.5 acceptor probes. Tb (TG): excitation: 349 nm, emission: 542±10 nm; Cy3.5 (CW): excitation: 578±8 nm, emission: 660±5 nm; FRET (TG): excitation: 349 nm, emission: 660±5 nm. Imaging conditions: TG: 400 GPI, 1 Ac, gain: 100 V. CW: 10 times 300 ms, gain: 6 V, lamp power: 15 W. Scale bars: 20 µm. DIC/PL overlay image can be found in **Supporting Figure S4**. Images of control experiments with the single probes and without probes can be found in **Supporting Figure S6**.

To further investigate the reason of Tb PL quenching when the fixed cells were immersed in TBS, we recorded Tb PL spectra in TBS, water, and HBSS. HBSS was selected because of bright Tb PL and FRET when previously used for live cell and *in vivo* imaging.[34] Because the dye fluorescence was not quenched when the fixed cells were immersed in TBS (*cf.* Cy3.5-to-AF647 FRET), we also measured Cy3.5 fluorescence spectra in the same buffer solutions. As expected from their performance in liquid-phase assays, both Tb and Cy3.5 showed only very minor PL quenching in buffers compared to water (**Supporting Figure S7a**). Thus, we added small amounts of formaldehyde (FA), which was used as standard cell fixative for these immuno-RCA assays, to the solutions in order to investigate its influence on PL quenching. For all aqueous solutions, FA resulted in significant Tb PL quenching, whereas Cy3.5 fluorescence was much less affected (**Supporting Figure S7b-d**). We therefore concluded that the standard fixative FA was responsible for Tb PL quenching when the cells were immersed in TBS. Only HBSS could circumvent a significant PL intensity decrease. A possible explanation would be a more efficient deactivation of FA by an accelerated formose reaction when using HBSS, which (unlike water and TBS) contains

glucose and Ca^{2+} and Mg^{2+} ions.[39,40] Future studies with different fixation materials and protocols and RCA initiation just before the measurements (instead of prior to fixation) will be necessary to fully understand the PL quenching and to adapt fixation toward optimal TG imaging conditions. The current actin immuno-RCA proof-of-concept study aimed at the actual demonstration of both CW dye-to-dye RCA-FRET and TG Tb-to-dye RCA-FRET and we decided to keep the same standard fixation conditions for both approaches and rather investigate the possibility of improving the TG imaging conditions by using HBSS instead of TBS.

As expected from the spectroscopy results, HBSS significantly improved the Tb PL intensities for imaging of the fixed HaCaT cells. When the cells were imaged during incubation of the detection oligos in TBS solution, no significant Tb PL signals could be detected in the FRET channel within 30 min after addition of the fluorescent probes (not shown). With HBSS probe incubation, a FRET signal could already be detected after five min and after 20 min the FRET signal was bright and remained relatively constant until 120 min (**Figure 4**). When comparing the Tb-to-Cy3.5 FRET images (TG detection of Cy3.5 PL upon excitation of Tb – **Figure 4**) with the Tb images (TG detection of Tb PL upon excitation of Tb – **Supporting Figure S8a**) and Cy3.5 images (CW detection of Cy3.5 PL upon excitation of Cy3.5 – **Supporting Figure S8b**), one can notice significant differences related to FRET-specific PL and to PL intensities. Owing to their short fluorescence lifetime (in the nanosecond range), Cy3.5 dyes can perform many excitation-emission cycles over time (photon flux) when using CW excitation. The micro- to millisecond PL lifetime of Tb requires pulsed excitation at a relatively low repetition rate (300 Hz in our case), which results in much fewer excitation-emission cycles over time. On the other hand, this lower photon flux of Tb results in significantly reduced photobleaching compared to Cy3.5. Therefore, Tb imaging can be performed over longer timescales to produce the same signal intensity but without increasing the background signals (due to TG detection). In general, it is difficult to directly compare TG and CW imaging with different fluorophores and the advantages or disadvantages of TG imaging also strongly depend on the fluorescence background of the samples. For samples with low autofluorescence, the higher photon flux of dyes is clearly beneficial because imaging becomes faster. For samples with high autofluorescence, signal-to-background ratios can be significantly improved when using TG imaging.[34] Here, we kept imaging conditions and image treatment for each detection channel (FRET, Tb, and Cy3.5) the same over the entire incubation time to compare the differences in signal and background over time (**Supporting Figure S9**). The Cy3.5 images

show the highest signals owing to their higher photon flux in CW imaging over 3 s in total (10 times 300 ms) but also the strongest background intensities. The Tb images present lower PL intensities than the Cy3.5 images owing to the lower photon flux during TG imaging over 3.3 s in total (1000 GPI at 300 Hz) but with much lower background intensities due to TG imaging. The TG-FRET images show the highest signal-to-background ratios because only donor-acceptor pairs inside the RCPs can result in FRET signals, which are therefore actin-specific. Thus, already at similar imaging time for CW and TG imaging, washing-free RCA-TG-FRET shows the best contrast between specific and non-specific PL signals.

Another interesting point of the possibility to image RCP-probe hybridization in real time (without washing steps) via background-free TG FRET is the dynamic range. By imaging the RCA process over time, as the RCPs are building up, highly abundant targets can be monitored before the sizes of the RCPs become so large that they start to coalesce. This feature would lead to clear and distinguishable target spots for a broad range of target concentrations without the necessity to adapt probe concentrations, which is the current method of increasing the dynamic range.[5] Considering that our proof-of-concept immuno-RCA approach resulted in many RCPs (high target abundance), the images after 5 min incubation are very interesting because at this initial state of RCP-probe hybridization, the single target spots become much better distinguishable than at longer incubation times and for all incubation times, the spot-distinction is easiest when using the RCP-specific FRET signals. Future studies of implementing *in situ* RCA-FRET into PLA will also investigate autofluorescence, total imaging time, dynamic range, and photobleaching in more detail.

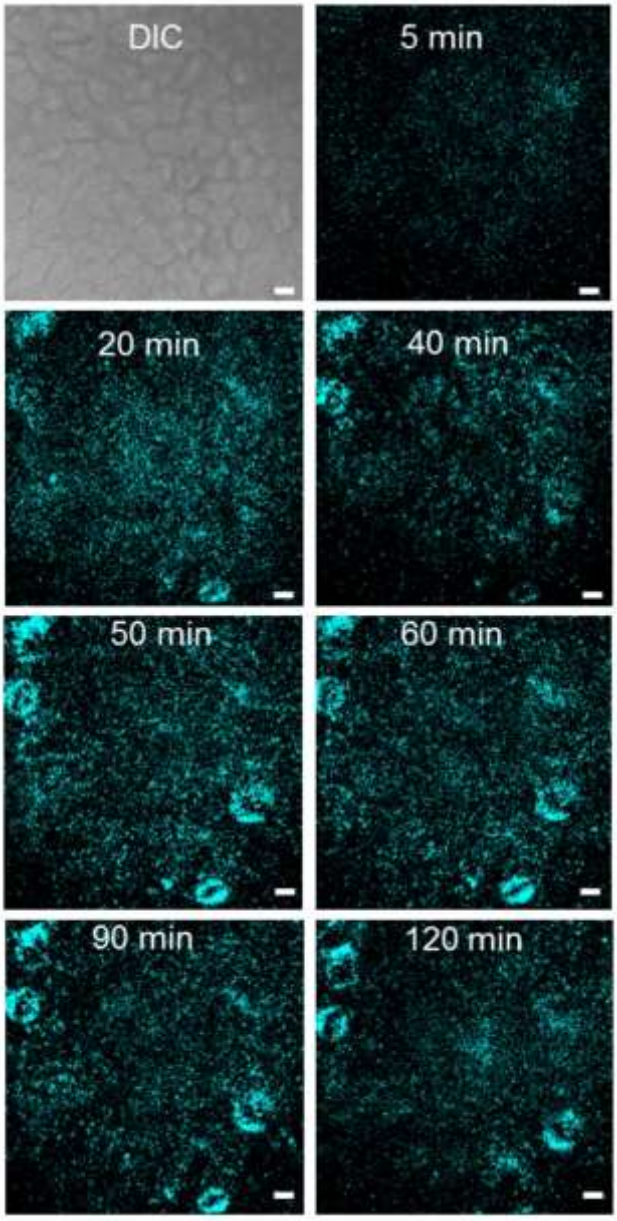

Figure 4: *In situ* RCA-FRET imaging of individual actin-activated immuno-RCPs on HaCaT cells during incubation at 36.5 °C with Tb donor probes and Cy3.5 acceptor probes in HBSS. PL images show the TG FRET detection channel (excitation: 349 nm; emission: 660±5 nm) after different incubation times. Scale bars: 10 µm. Imaging conditions: TG: 1000 GPI, 1 Ac, gain: 100 V. Tb (TG) and Cy3.5 (CW) can be found in **Supporting Figure S8**.

Although following the RCP-probe hybridization over time is certainly an interesting capability of TG FRET, we found that removal of HBSS from the cells before imaging resulted in even brighter imaging signals (**Figure 5**). While the imaging results looked very similar to those accomplished with TBS and three washing steps (*cf.* **Figure 3a**), the increased signal intensities allowed us to

further decrease the experimental time to 15 min of incubation, removal of the HBSS, and direct target-specific TG-FRET imaging without any washing steps.

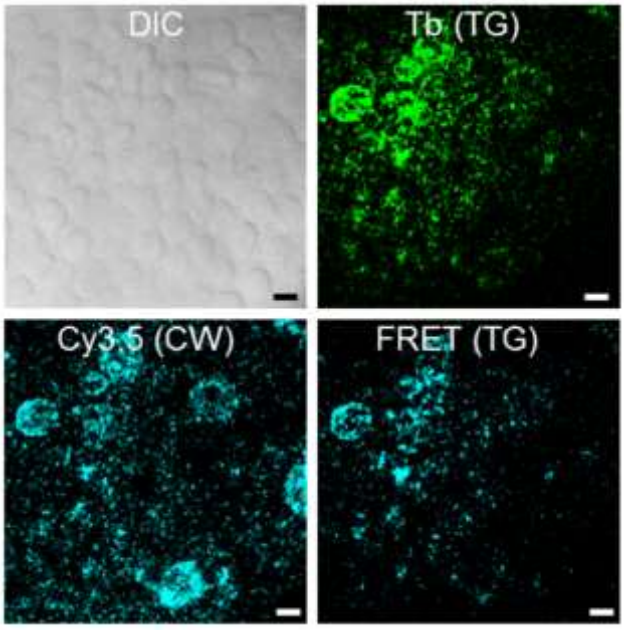

Figure 5: *In situ* RCA-FRET imaging of individual actin-specific immuno-RCPs on HaCaT cells incubated with Tb donor probes and Cy3.5 acceptor probes. Tb (TG): excitation: 349 nm, emission: 542±10 nm; Cy3.5 (CW): excitation: 578±8 nm, emission: 660±5 nm; FRET (TG): excitation: 349 nm, emission: 660±5 nm. Imaging conditions: TG: 1000 GPI, 1 Ac, gain: 100 V. CW: 10 times 300 ms, gain: 6 V, lamp power: 15 W. Scale bars: 20 µm.

CONCLUSIONS

Using β-actin-specific immuno-RCA on fixed HaCaT cells as a well-established model system for *in situ* PLA, we could demonstrate RCA-FRET for two different FRET approaches, namely dye-to-dye CW FRET and Tb-to-dye TG FRET. Because FRET can only be accomplished when both donor and acceptor hybridize to the same RCP, the FRET approach does not require any separation of freely diffusing donor and acceptor DNA probes from the samples and can efficiently distinguish target-specific RCP-probe hybridization from non-specific attachment to the cells. Therefore, *in situ* imaging of individual RCPs can be performed without any washing steps, which makes this approach significantly faster and simpler than conventional *in situ* RCA. While CW dye-to-dye FRET was relatively straightforward to implement because fixation and *in situ* RCA conditions were already adapted to dye-based fluorescence imaging, TG Tb-to-dye FRET appeared more challenging because of Tb PL quenching when the Tb-DNA probes were incubated with the fixed

cells. This PL quenching was caused by FA used for cell fixation and future studies will focus on optimizing cell fixation protocols toward Tb-DNA probes. On the other hand, replacing TBS buffer by HBSS resulted in significantly less Tb PL quenching, which allowed us to follow the Tb and dye probe hybridization to the single RCPs in real time during incubation. Removing the buffer (HBSS or TBS) from the fixed cells directly before imaging improved the Tb PL intensity even further and we could accomplish bright RCA-TG-FRET after only 15 minutes of probe incubation with the cells and subsequent buffer removal without any washing steps. The improved signal-to-background ratios of TG and TG-FRET imaging (compared to CW imaging) underline the significant benefits that lanthanide complexes can bring to advanced high-contrast PL imaging.[9,34,37,41–46] Notably, lanthanide-based TG PL imaging of fixed cells or tissues is not common and considering that the well-established solution-phase TG-FRET assays have only recently been implemented into advanced live cell and *in vivo* imaging, we can anticipate that the same performance can be expected for carefully optimized TG imaging on fixed cells. Similar to immunohistochemistry, the performance of *in situ* PLA depends on the fixation and pretreatment conditions, the applied antibody-DNA probes, and the careful adaption of assay components and their concentrations, which are important optimization steps that are beyond our *in situ* RCA-FRET proof-of-concept study.

With the important *in situ* RCA-FRET demonstration at hand, future studies will focus on the implementation into *in situ* PLA and investigate optimized experimental conditions to accomplish the highest possible signal-to-background ratios for both CW and TG FRET. Moreover, in particular TG FRET with Tb donors provides significant advantages concerning multiplexing (both spectral and temporal),[9,15–17,20,21,36,47,48] which may extend the current experimental limit of three colors for *in situ* PLA[5,6] to much higher-order multiplexing. The other main advantage of TG FRET is the efficient suppression of autofluorescence and therefore *in situ* PLA-TG-FRET would be particularly interesting to exploit in clinical tissue sections. Also *in vivo* PLA would be an interesting field to investigate because washing is usually not possible *in vivo* and the washing-free FRET approach may provide ideal conditions for *in vivo* PLA imaging. In summary, the capability of implementing FRET into *in situ* PLA offers many possible advantages and our proof-of-principle results present only an initiator to a new approach of *in situ* PLA that may find useful application in biological and clinical research and diagnostics.

ASSOCIATED CONTENT

Supporting Information

Chemical structures of the lanthanide complexes used for TG imaging; TG and CW images of *in situ* RCA in HaCaT cells detected with three different organic dyes and three different lanthanide complexes; overlay images of DIC and PL for CW and TG RCA-FRET; determination of signal-to-background ratios; *in situ* RCA imaging with single Tb and Cy3.5 probes and without probes; Tb and Cy3.5 PL spectra in different aqueous solutions with and without FA; images of RCP-probe hybridization over time in Tb and Cy3.5 detection channels.

ACKNOWLEDGEMENTS

We thank Lumiphore, Inc. for the gift of Lumi4 reagents. This work was partially funded by the European Commission (Marie Skłodowska-Curie Actions, Individual Fellowship of Laura Francés-Soriano), the French National Research Agency (ANR projects "PhenX" and "Neutrinos" and Labex "SynOrg"), the Région Normandie (Chaire d'Excellence "COBRA-FRET"), the Institut Universitaire de France (IUF), the Swedish Research Council, and the Swedish Cancer Foundation.

REFERENCES

(1) Smith, M. A.; Hall, R.; Fisher, K.; Haake, S. M.; Khalil, F.; Schabath, M. B.; Vuaroqueaux, V.; Fiebig, H.-H.; Altiok, S.; Chen, Y. A.; Haura, E. B. Annotation of Human Cancers with EGFR Signaling-Associated Protein Complexes Using Proximity Ligation Assays. *Sci Signal* **2015**, *8* (359), ra4. https://doi.org/10.1126/scisignal.2005906.

(2) Ricardo, S.; Marcos-Silva, L.; Pereira, D.; Pinto, R.; Almeida, R.; Söderberg, O.; Mandel, U.; Clausen, H.; Felix, A.; Lunet, N.; David, L. Detection of Glyco-Mucin Profiles Improves Specificity of MUC16 and MUC1 Biomarkers in Ovarian Serous Tumours. *Mol Oncol* **2015**, *9* (2), 503–512. https://doi.org/10.1016/j.molonc.2014.10.005.

(3) Jarvius, M.; Paulsson, J.; Weibrecht, I.; Leuchowius, K.-J.; Andersson, A.-C.; Wählby, C.; Gullberg, M.; Botling, J.; Sjöblom, T.; Markova, B.; Ostman, A.; Landegren, U.; Söderberg, O. In Situ Detection of Phosphorylated Platelet-Derived Growth Factor Receptor Beta Using a Generalized Proximity Ligation Method. *Mol Cell Proteomics* **2007**, *6* (9), 1500–1509. https://doi.org/10.1074/mcp.M700166-MCP200.

(4) Söderberg, O.; Gullberg, M.; Jarvius, M.; Ridderstråle, K.; Leuchowius, K.-J.; Jarvius, J.; Wester, K.; Hydbring, P.; Bahram, F.; Larsson, L.-G.; Landegren, U. Direct Observation of Individual Endogenous Protein Complexes in Situ by Proximity Ligation. *Nat Methods* **2006**, *3* (12), 995–1000. https://doi.org/10.1038/nmeth947.

(5) Clausson, C.-M.; Allalou, A.; Weibrecht, I.; Mahmoudi, S.; Farnebo, M.; Landegren, U.; Wählby, C.; Söderberg, O. Increasing the Dynamic Range of in Situ PLA. *Nat. Methods* **2011**, *8* (11), 892–893. https://doi.org/10.1038/nmeth.1743.

(6) Leuchowius, K.-J.; Clausson, C.-M.; Grannas, K.; Erbilgin, Y.; Botling, J.; Zieba, A.; Landegren, U.; Söderberg, O. Parallel Visualization of Multiple Protein Complexes in Individual Cells in Tumor Tissue. *Mol. Cell Proteomics* **2013**, *12* (6), 1563–1571. https://doi.org/10.1074/mcp.O112.023374.

(7) Klaesson, A.; Grannas, K.; Ebai, T.; Heldin, J.; Koos, B.; Leino, M.; Raykova, D.; Oelrich, J.; Arngården, L.; Söderberg, O.; Landegren, U. Improved Efficiency of in Situ Protein Analysis by Proximity Ligation Using UnFold Probes. *Sci Rep* **2018**, *8* (1), 5400. https://doi.org/10.1038/s41598-018-23582-1.

(8) *FRET - Förster Resonance Energy Transfer: From Theory to Applications*; Medintz, I., Hildebrandt, N., Eds.; Wiley VCH: Weinheim, 2013.
(9) Zwier, J. M.; Hildebrandt, N. Time-Gated FRET Detection for Multiplexed Biosensing. In *Reviews in Fluorescence 2016*; Geddes, CD, Ed.; Reviews in Fluorescence; 2017; pp 17–43. https://doi.org/10.1007/978-3-319-48260-6_3.
(10) Hemmila, I. LANCE^{TM}: Homogeneous Assay Platform for HTS. *J. Biomol. Screen.* **1999**, *4* (6), 303–307. https://doi.org/10.1177/108705719900400604.
(11) Mathis, G. HTRF® Technology. *J. Biomol. Screen.* **1999**, *4* (6), 309–313. https://doi.org/10.1177/108705719900400605.
(12) LANCE TR-FRET|PerkinElmer https://www.perkinelmer.com/fr/category/lance-tr-fret (accessed Sep 24, 2020).
(13) HTRF technology | Cisbio https://fr.cisbio.eu/content/htrf-technology/ (accessed Sep 24, 2020).
(14) TRACE Technology - B·R·A·H·M·S KRYPTOR Analyzers https://www.brahms-instruments.com/trace-technology.html (accessed Sep 24, 2020).
(15) Jin, Z.; Geißler, D.; Qiu, X.; Wegner, K. D.; Hildebrandt, N. A Rapid, Amplification-Free, and Sensitive Diagnostic Assay for Single-Step Multiplexed Fluorescence Detection of MicroRNA. *Angew. Chem. Int. Ed. Engl.* **2015**, *54* (34), 10024–10029. https://doi.org/10.1002/anie.201504887.
(16) Qiu, X.; Hildebrandt, N. Rapid and Multiplexed MicroRNA Diagnostic Assay Using Quantum Dot-Based Förster Resonance Energy Transfer. *ACS Nano* **2015**, *9* (8), 8449–8457. https://doi.org/10.1021/acsnano.5b03364.
(17) Qiu, X.; Guo, J.; Jin, Z.; Petreto, A.; Medintz, I. L.; Hildebrandt, N. Multiplexed Nucleic Acid Hybridization Assays Using Single-FRET-Pair Distance-Tuning. *Small* **2017**, *13* (25). https://doi.org/10.1002/smll.201700332.
(18) Qiu, X.; Xu, J.; Guo, J.; Yahia-Ammar, A.; Kapetanakis, N.-I.; Duroux-Richard, I.; Unterluggauer, J. J.; Golob-Schwarzl, N.; Regeard, C.; Uzan, C.; Gouy, S.; DuBow, M.; Haybaeck, J.; Apparailly, F.; Busson, P.; Hildebrandt, N. Advanced MicroRNA-Based Cancer Diagnostics Using Amplified Time-Gated FRET. *Chem. Sci.* **2018**, *9* (42), 8046–8055. https://doi.org/10.1039/c8sc03121e.
(19) Dekaliuk, M.; Qiu, X.; Troalen, F.; Busson, P.; Hildebrandt, N. Discrimination of the V600E Mutation in BRAF by Rolling Circle Amplification and Förster Resonance Energy Transfer. *ACS Sens.* **2019**, *4* (10), 2786–2793. https://doi.org/10.1021/acssensors.9b01420.
(20) Xu, J.; Guo, J.; Golob-Schwarzl, N.; Haybaeck, J.; Qiu, X.; Hildebrandt, N. Single-Measurement Multiplexed Quantification of MicroRNAs from Human Tissue Using Catalytic Hairpin Assembly and Förster Resonance Energy Transfer. *ACS Sens.* **2020**, *5* (6), 1768–1776. https://doi.org/10.1021/acssensors.0c00432.
(21) Qiu, X.; Guo, J.; Xu, J.; Hildebrandt, N. Three-Dimensional FRET Multiplexing for DNA Quantification with Attomolar Detection Limits. *J. Phys. Chem. Lett.* **2018**, *9* (15), 4379–4384. https://doi.org/10.1021/acs.jpclett.8b01944.
(22) Zhou, F.; Li, B.; Ma, J. A Linear DNA Probe as an Alternative to a Molecular Beacon for Improving the Sensitivity of a Homogenous Fluorescence Biosensing Platform for DNA Detection Using Target-Primed Rolling Circle Amplification. *RSC Adv.* **2014**, *5* (6), 4019–4025. https://doi.org/10.1039/C4RA14467H.
(23) Wu, X.; Zhu, S.; Huang, P.; Chen, Y. Highly Specific Quantification of MicroRNA by Coupling Probe-Rolling Circle Amplification and Förster Resonance Energy Transfer. *Anal. Biochem.* **2016**, *502*, 16–23. https://doi.org/10.1016/j.ab.2016.03.001.
(24) Schweitzer, B.; Wiltshire, S.; Lambert, J.; O'Malley, S.; Kukanskis, K.; Zhu, Z.; Kingsmore, S. F.; Lizardi, P. M.; Ward, D. C. Immunoassays with Rolling Circle DNA Amplification: A Versatile Platform for Ultrasensitive Antigen Detection. *Proc Natl Acad Sci U S A* **2000**, *97* (18), 10113–10119. https://doi.org/10.1073/pnas.170237197.
(25) Xu, J.; Corneillie, T. M.; Moore, E. G.; Law, G. L.; Butlin, N. G.; Raymond, K. N. Octadentate Cages of Tb(III) 2-Hydroxyisophthalamides: A New Standard for Luminescent Lanthanide Labels. *J. Am. Chem. Soc.* **2011**, *133* (49), 19900–19910. https://doi.org/10.1021/ja2079898.
(26) Kovacs, D.; Kiraev, S. R.; Phipps, D.; Orthaber, A.; Borbas, K. E. Eu(III) and Tb(III) Complexes of Octa- and Nonadentate Macrocyclic Ligands Carrying Azide, Alkyne, and Ester Reactive Groups. *Inorg. Chem.* **2020**, *59* (1), 106–117. https://doi.org/10.1021/acs.inorgchem.9b01576.
(27) Hildebrandt, N. How to Apply FRET: From Experimental Design to Data Analysis. In *FRET - Förster resonance energy transfer: from theory to applications*; Medintz, I., Hildebrandt, N., Eds.; Wiley VCH: Weinheim, 2013; pp 105–164.

(28) Sanborn, M. E.; Connolly, B. K.; Gurunathan, K.; Levitus, M. Fluorescence Properties and Photophysics of the Sulfoindocyanine Cy3 Linked Covalently to DNA. *J. Phys. Chem. B* **2007**, *111* (37), 11064–11074. https://doi.org/10.1021/jp072912u.
(29) Leuchowius, K.-J.; Weibrecht, I.; Söderberg, O. In Situ Proximity Ligation Assay for Microscopy and Flow Cytometry. *Curr Protoc Cytom* **2011**, *Chapter 9*, Unit 9.36. https://doi.org/10.1002/0471142956.cy0936s56.
(30) Qiu, X.; Guittet, O.; Mingoes, C.; El Banna, N.; Huang, M.-E.; Lepoivre, M.; Hildebrandt, N. Quantification of Cellular Deoxyribonucleoside Triphosphates by Rolling Circle Amplification and Förster Resonance Energy Transfer. *Anal. Chem.* **2019**, *91* (22), 14561–14568. https://doi.org/10.1021/acs.analchem.9b03624.
(31) Mandelkern, M.; Elias, J. G.; Eden, D.; Crothers, D. M. The Dimensions of DNA in Solution. *J. Mol. Biol.* **1981**, *152* (1), 153–161. https://doi.org/10.1016/0022-2836(81)90099-1.
(32) Schnell, S. A.; Staines, W. A.; Wessendorf, M. W. Reduction of Lipofuscin-like Autofluorescence in Fluorescently Labeled Tissue. *J. Histochem. Cytochem.* **1999**, *47* (6), 719–730. https://doi.org/10.1177/002215549904700601.
(33) Viegas, M. S.; Martins, T. C.; Seco, F.; do Carmo, A. An Improved and Cost-Effective Methodology for the Reduction of Autofluorescence in Direct Immunofluorescence Studies on Formalin-Fixed Paraffin-Embedded Tissues. *Eur. J. Histochem.* **2007**, *51* (1), 59–66.
(34) Cardoso Dos Santos, M.; Colin, I.; Santos, G. R. D.; Susumu, K.; Demarque, M.; Medintz, I. L.; Hildebrandt, N. Time-Gated FRET Nanoprobes for Autofluorescence-Free Long-Term In Vivo Imaging of Developing Zebrafish. *Advanced Materials* **2020**, *32* (39), 2003912. https://doi.org/10.1002/adma.202003912.
(35) Rajapakse, H. E.; Gahlaut, N.; Mohandessi, S.; Yu, D.; Turner, J. R.; Miller, L. W. Time-Resolved Luminescence Resonance Energy Transfer Imaging of Protein-Protein Interactions in Living Cells. *Proc. Natl. Acad. Sci. U.S.A.* **2010**, *107* (31), 13582–13587. https://doi.org/10.1073/pnas.1002025107.
(36) Hildebrandt, N.; Wegner, K. D.; Algar, W. R. Luminescent Terbium Complexes: Superior Förster Resonance Energy Transfer Donors for Flexible and Sensitive Multiplexed Biosensing. *Coord. Chem. Rev.* **2014**, *273* (SI), 125–138. https://doi.org/10.1016/j.ccr.2014.01.020.
(37) Chen, T.; Pham, H.; Mohamadi, A.; Miller, L. W. Single-Chain Lanthanide Luminescence Biosensors for Cell-Based Imaging and Screening of Protein-Protein Interactions. *iScience* **2020**, *23* (9). https://doi.org/10.1016/j.isci.2020.101533.
(38) Bhuckory, S.; Wegner, K. D.; Qiu, X.; Wu, Y.-T.; Jennings, T. L.; Incamps, A.; Hildebrandt, N. Triplexed CEA-NSE-PSA Immunoassay Using Time-Gated Terbium-to-Quantum Dot FRET. *Molecules* **2020**, *25* (16). https://doi.org/10.3390/molecules25163679.
(39) Kingsbury, F. B. Note on the Effect of Glucose on the Condensation of Formaldehyde I. the Determination of Urinary Sugar by This Principle. *J. Biol. Chem.* **1927**, *75* (1), 241–245.
(40) Matsumoto, T.; Inoue, S. Formose Reactions. Part 3. Selective Formose Reaction Catalyzed by Organic Bases. *J. Chem. Soc., Perkin Trans. 1* **1982**, No. 0, 1975–1979. https://doi.org/10.1039/P19820001975.
(41) Carro-Temboury, M. R.; Arppe, R.; Hempel, C.; Vosch, T.; Sørensen, T. J. Creating Infinite Contrast in Fluorescence Microscopy by Using Lanthanide Centered Emission. *PLOS ONE* **2017**, *12* (12), e0189529. https://doi.org/10.1371/journal.pone.0189529.
(42) Moreno Delgado, D.; Møller, T. C.; Ster, J.; Giraldo, J.; Maurel, D.; Rovira, X.; Scholler, P.; Zwier, J. M.; Perroy, J.; Durroux, T.; Trinquet, E.; Prezeau, L.; Rondard, P.; Pin, J.-P. Pharmacological Evidence for a Metabotropic Glutamate Receptor Heterodimer in Neuronal Cells. *Elife* **2017**, *6*. https://doi.org/10.7554/eLife.25233.
(43) Arppe-Tabbara, R.; Carro-Temboury, M. R.; Hempel, C.; Vosch, T.; Sørensen, T. J. Luminescence from Lanthanide(III) Ions Bound to the Glycocalyx of Chinese Hamster Ovary Cells. *Chemistry* **2018**, *24* (46), 11885–11889. https://doi.org/10.1002/chem.201802799.
(44) Parker, D.; Fradgley, J. D.; Zwier, J. M.; Starck, M.; Pal, R.; Lamarque, L. Synthesis and Evaluation of Europium Complexes That Switch On Luminescence in Lysosomes of Living Cells. *Chemistry* **2020**. https://doi.org/10.1002/chem.202003992.
(45) Afsari, H. S.; Dos Santos, M. C.; Linden, S.; Chen, T.; Qiu, X.; Henegouwen, P. M. P. van B. E.; Jennings, T. L.; Susumu, K.; Medintz, I. L.; Hildebrandt, N.; Miller, L. W. Time-Gated FRET Nanoassemblies for Rapid and Sensitive Intra- and Extracellular Fluorescence Imaging. *Sci. Adv.* **2016**, *2* (6), e1600265. https://doi.org/10.1126/sciadv.1600265.
(46) Cho, U.; Riordan, D. P.; Ciepla, P.; Kocherlakota, K. S.; Chen, J. K.; Harbury, P. B. Ultrasensitive Optical Imaging with Lanthanide Lumiphores. *Nat. Chem. Biol.* **2018**, *14* (1), 15–21. https://doi.org/10.1038/nchembio.2513.

(47) Geissler, D.; Stufler, S.; Loehmannsroeben, H.-G.; Hildebrandt, N. Six-Color Time-Resolved Forster Resonance Energy Transfer for Ultrasensitive Multiplexed Biosensing. *J. Am. Chem. Soc.* **2013**, *135* (3), 1102–1109. https://doi.org/10.1021/ja310317n.
(48) Guo, J.; Mingoes, C.; Qiu, X.; Hildebrandt, N. Simple, Amplified, and Multiplexed Detection of MicroRNAs Using Time-Gated FRET and Hybridization Chain Reaction. *Anal. Chem.* **2019**, *91* (4), 3101–3109. https://doi.org/10.1021/acs.analchem.8b05600.